

How Analytic Choices Can Affect the Extraction of Electromagnetic Form Factors from Elastic Electron Scattering Cross Section Data

Scott K. Barcus, Douglas W. Higinbotham, and Randall E. McClellan
Jefferson Lab, Newport News, VA 23606

Scientists often try to incorporate prior knowledge into their regression algorithms, such as a particular analytic behavior or a known value at a kinematic endpoint. Unfortunately, there is often no unique way to make use of this prior knowledge, and thus, different analytic choices can lead to very different regression results from the same set of data. To illustrate this point in the context of the proton electromagnetic form factors, we use the Mainz elastic data with its 1422 cross section points and 31 normalization parameters. Starting with a complex unbound non-linear regression, we will show how the addition of a single theory-motivated constraint removes an oscillation from the magnetic form factor and shifts the extracted proton charge radius. We then repeat both regressions using the same algorithm, but with a rebinned version of the Mainz dataset. These examples illustrate how analytic choices, such as the function that is being used or even the binning of the data, can dramatically affect the results of a complex regression. These results also demonstrate why it is critical when using regression algorithms to have either a physical model in mind or a firm mathematical basis to avoid confirmation bias.

Keywords: form factors; proton radius; confirmation bias; regression; robust methods

I. INTRODUCTION

Silberzahn *et al.* [1] points out that there is often little appreciation for how different analytic strategies can affect a reported result. In this work, we illustrate how analytic choices can impact the extraction of the electromagnetic form factors and the associated charge radii from electron scattering data. These extractions are frequently done with complex non-linear regression algorithms and tend to make use of prior information about the limiting behavior of the electromagnetic form factors through the use of floating normalization parameters. Also, while many tend to look at all regressions as being the same, in fact there are many different types of regressions such as descriptive, predictive, and explanatory.

A descriptive model is used to capture the features of a dataset in a compact manner without reliance on an underlying theory. A predictive model is any statistical model which tries to generalize beyond the data that is being fitted. Finally, explanatory modeling takes a theory based model and tests that model hypothesis by applying it to data. Further details about these differences can be found in Ref. [2]. Though the type of regression model being developed is not always clearly stated, it is yet another choice that affects how scientists design their regression algorithms.

II. PROTON ELASTIC SCATTERING

There has been renewed interest in proton elastic scattering data due to muonic hydrogen Lamb shift results that determined the charge radius of the proton to be 0.84078(39) fm [3, 4], a result in stark contrast to the CODATA-2014 recommended value of 0.8751(61) fm [5]. This systematic difference was known as the proton radius puzzle [6–8].

In the plane-wave Born approximation, the cross section for elastic electron scattering on a proton is given by:

$$\sigma = \sigma_{\text{Mott}} \times \left[\frac{G_E^2(Q^2) + \tau G_M^2(Q^2)}{1 + \tau} + 2\tau G_M^2(Q^2) \tan^2\left(\frac{\theta}{2}\right) \right], \quad (1)$$

where σ_{Mott} is the Mott cross section, G_E and G_M are the electric and magnetic Sachs form factors, $\tau = \frac{Q^2}{4m_p^2}$, $Q^2 = 4E_{\text{Beam}}E' \sin^2\left(\frac{\theta}{2}\right)$, E_{Beam} is the energy of the electron beam, E' is the energy of the outgoing electron, θ is the scattering angle of the outgoing electron, and m_p is the mass of the proton.

The proton charge radius, r_p , is extracted from the cross sections by determining the slope of the electric form factor, G_E , in the limit of four-moment transfer, Q^2 , approaching zero [9]:

$$r_p \equiv \left(-6 \left. \frac{dG_E(Q^2)}{dQ^2} \right|_{Q^2=0} \right)^{1/2}. \quad (2)$$

Since the scattering data is measured at finite Q^2 , an extrapolation is required to extract the charge radius. Authors have taken many different approaches to this extraction, yielding different outcomes [10–18].

III. REGRESSIONS

To illustrate how analytic choice can strongly affect the extracted radius, we first use the Mainz dataset of 1422 cross section points along with its 31 normalization

parameters [19]. This dataset is fit with an unbound complex non-linear regression following the procedure described in Ref. [19, 20] where the form factors are parameterized in terms of polynomials:

$$G_{E,\text{polynomial}}(a_i^E, Q^2) = 1 + \sum_{i=1}^n a_i^E Q^{2i} \quad \text{and} \quad (3)$$

$$G_{M,\text{polynomial}}(a_i^M, Q^2) = \mu_p \left(1 + \sum_{i=1}^n a_i^M Q^{2i} \right), \quad (4)$$

where μ_p is the magnetic moment of the proton and n is the order of the polynomial.

For these regressions, we will do a weighted least squares minimization with a χ^2 function defined as follows:

$$\chi^2 = \sum_{p=1}^{p_{\max}} \left(\frac{\sigma_{\text{Model}}(E_p, \theta_p) - \sigma_p \cdot \text{norm}A_p \cdot \text{norm}B_p}{\Delta\sigma_p \cdot \text{norm}A_p \cdot \text{norm}B_p} \right)^2, \quad (5)$$

where for each data point p there is a cross-section, σ_p , with energy E_p , angle θ_p , and normalization parameters $\text{norm}A$ and $\text{norm}B$ as shown in Table I. As was done in the original Mainz fits, the normalization parameters are allowed to float freely.

We will then repeat this same regression adding one requirement: that the electromagnetic form factors be ‘‘completely monotone’’ functions. These are functions f that possess derivatives f^n of all orders such that $(-1)^n f^n(x) \geq 0, x > 0$ (i.e. the terms of the polynomial have successively alternating signs) [21]. This seemingly simple constraint imposes an analytic behavior to the form factors that is constant with nuclear physics calculations such as chiral effective field theory [22]. In statistics terms, adding the condition that the function be completely monotone would be classified as creating a robust regression model [23]. Robust regression models are designed to not be unduly affected by outliers; whereas least squares estimates are highly sensitive to outlying points as illustrated in Appendix A.

As a further check of how sensitive these two functions are to the handling of the data in the fit, we use the rebinned version of the Mainz data that is provided in the supplemental material of Ref. [13]. These authors carefully rebinned and re-weighted the full Mainz dataset and provided a new set of 658 cross section points, though with the same 31 normalization parameters as the original set. By simply replacing the original Mainz dataset with this set, we can repeat our bound and unbound regressions. Ideally, these regression models would have been carefully developed prior to obtaining the experimental data, as was done by the PRad collaboration [24]; otherwise, one must be exceedingly careful to avoid confirmation bias though the rigorous use of model selection techniques [25, 26].

While regressions that are linear in terms can be solved exactly, this is not the case with non-linear regressions

where algorithms can converge in a local or non-physical minimum; thus choosing reasonable initialization parameters is an important step when developing non-linear regression algorithms. To have reasonable initialization parameters for our complex non-linear regressions, we first performed a regression with dipole functions for G_E and G_M to determine the values of our initialization parameters.

As noted in the work of Bernauer *et al.* [20], knowledge of the absolute value of cross sections is limited by the determination of the absolute luminosity which in turn is limited by the uncertainty of the target thickness and beam current. In order to compensate for these uncertainties, the normalization parameters were introduced to the original fits of this data constrained only by our prior knowledge of the value of the charge and magnetic form factors in the limit of $Q^2 = 0$. This brings a model dependence to the analysis that is not easily understood. These parameters are taken in combinations to link sets of data together, with the final value of each cross section point defined by:

$$\sigma_{exp} = \sigma_p \cdot \text{norm}A_p \cdot \text{norm}B_p, \quad (6)$$

where $\text{norm}A_p$ and $\text{norm}B_p$ are the two normalization parameters associated with that data point. A complete list of the 31 different normalization parameters, N_j , that are taken in 34 unique combinations for the 1422 points, is shown in Table I. Further details of how these parameters connect to each of the 1422 cross section points can be found in the supplemental material of Bernauer *et al.* [20].

In Table II and Table III we show the results of fitting with both the bound and unbound regressions for the 1422 Mainz cross section points and the rebinned 658 Mainz cross section points respectively. The regression results and residuals are shown graphically in Fig. 1 (1422 Mainz cross section points) and Fig. 2 (rebinning 658 Mainz cross section points), where for clarity we have divided σ_{exp} by σ_{dipole} , where σ_{dipole} is simply Eq. 1 with standard dipole form factors:

$$G_{E,\text{dipole}}(Q^2) = \left(1 + \frac{Q^2}{0.71 \text{ GeV}^2} \right)^{-2}, \quad (7)$$

$$G_{M,\text{dipole}}(Q^2) = \mu_p \left(1 + \frac{Q^2}{0.71 \text{ GeV}^2} \right)^{-2}. \quad (8)$$

These results show that even just rebinning the data can shift the result of a high-order polynomial regression significantly.

IV. MODEL SELECTION

For a fixed number of fit parameters, the unbound regressions presented in this work will always have a total

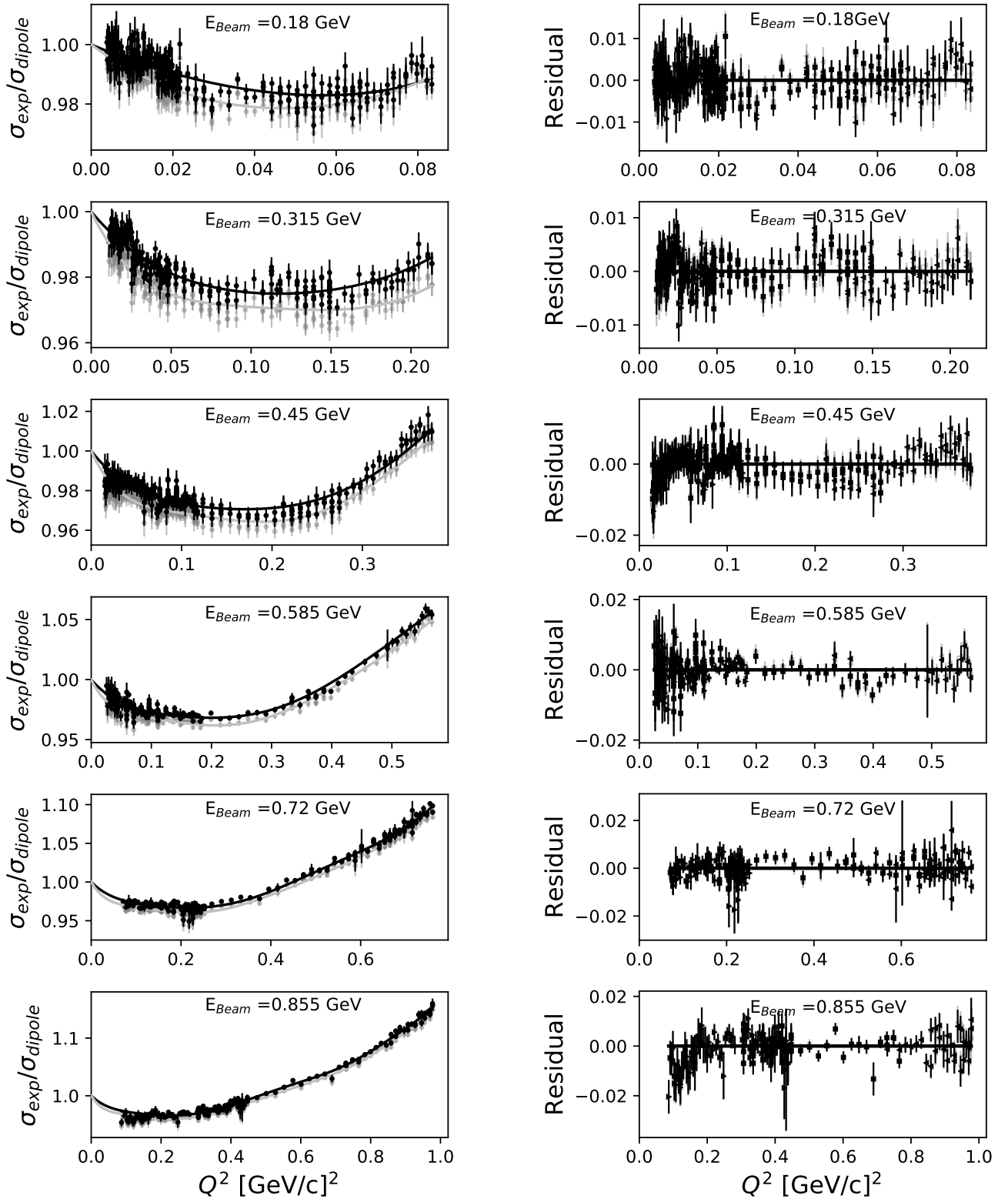


FIG. 1. Shown are the 1422 Mainz cross section points analyzed with the two different analytic choices. The grey points were analyzed using an unbound eleventh order polynomial regression in G_E and G_M while the black points used a bound eleventh order polynomial regression constrained to be continuously monotone as one would expect from chiral effective field theory. The systematic difference in the location of the points is due to how the 31 normalization parameters in the fit change based on the choice of using either the unbound or bound functions in the regression. While these means are different, the residuals of the fits to their respective functions are quite similar.

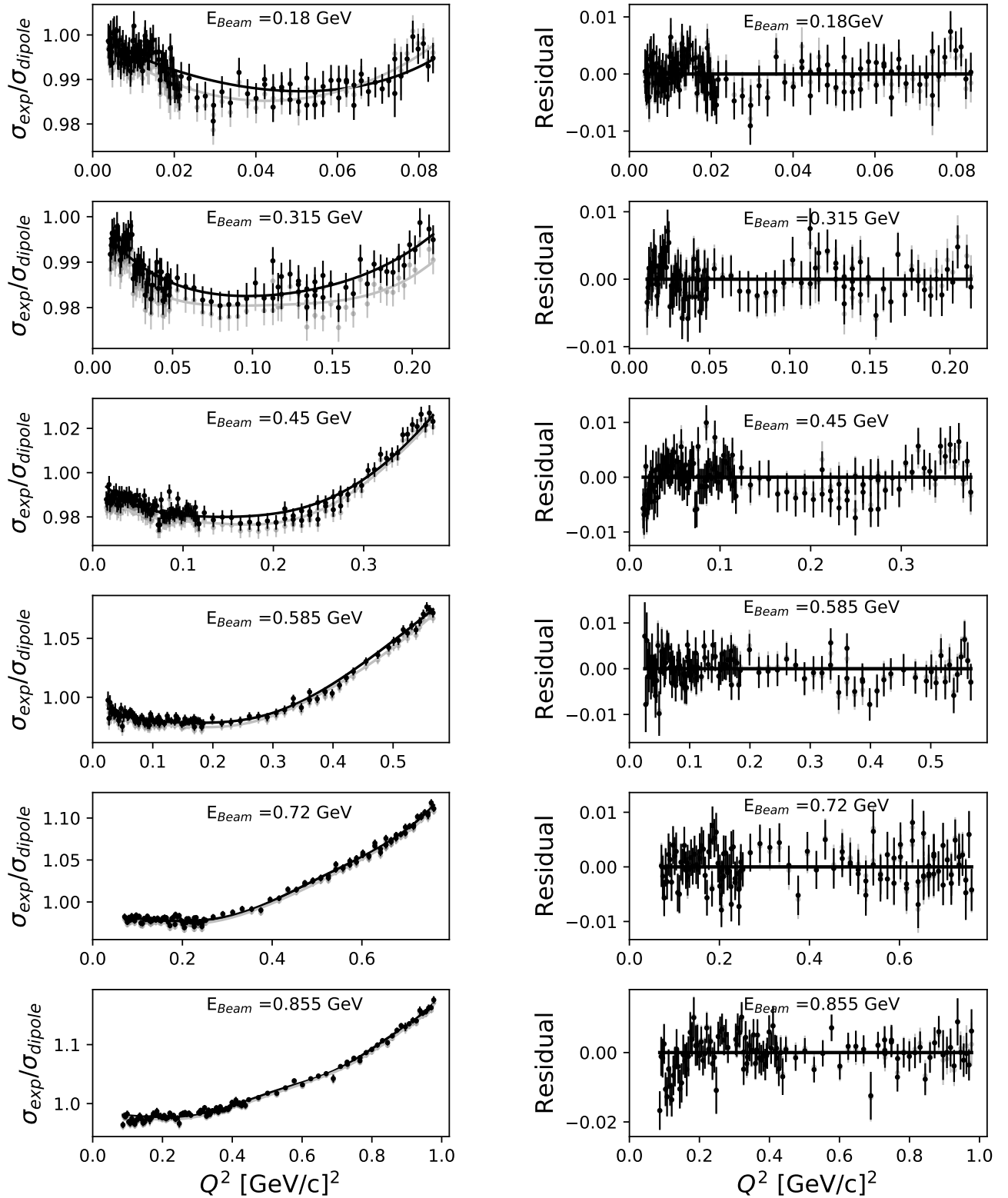


FIG. 2. Shown are the rebinned 658 Mainz cross section points analyzed with the two different analytic choices. The grey points were analyzed using an unbound eleventh order polynomial regression in G_E and G_M while the black points used a bound eleventh order polynomial regression constrained to be continuously monotone as one would expect from chiral effective field theory. The systematic difference in the location of the points is due to how the 31 normalization parameters in the fit change based on the choice of using either the unbound or bound functions in the regression. While these means are again very different for the two fits, the residuals of the fits to their respective functions are amazingly similar.

TABLE I. Shown are the 34 different combinations of the 31 normalization parameters, N_j , found in Ref. [20] which link the data together. Also shown are the number of data points and the Q^2 range of each dataset.

Energy	Spec.	$normA$	$normB$	Points	Q^2 Range [GeV ²]
180 MeV	B	N ₁	N ₃	106	0.0038 – 0.0129
	B	N ₁	N ₄	41	0.0101 – 0.0190
	A	N ₃	-	102	0.0112 – 0.0658
	B	N ₁	N ₅	19	0.0190 – 0.0295
	C	N ₂	N ₄	38	0.0421 – 0.0740
	C	N ₂	N ₅	17	0.0740 – 0.0834
315 MeV	B	N ₆	N ₉	104	0.0111 – 0.0489
	A	N ₇	N ₉	38	0.0430 – 0.1391
	A	N ₉	-	40	0.0479 – 0.1441
	C	N ₈	N ₉	62	0.1128 – 0.2131
450 MeV	B	N ₁₀	N ₁₃	77	0.0152 – 0.0572
	B	N ₁₀	N ₁₅	52	0.0572 – 0.1175
	A	N ₁₃	-	42	0.0586 – 0.2663
	B	N ₁₀	N ₁₄	17	0.0589 – 0.0851
	A	N ₁₁	N ₁₃	36	0.0670 – 0.2744
	C	N ₁₂	N ₁₅	50	0.2127 – 0.3767
	A	N ₁₄	-	2	0.2744 – 0.2744
585 MeV	B	N ₁₆	N ₁₈	41	0.0255 – 0.0433
	B	N ₁₆	N ₁₉	47	0.0433 – 0.1110
	A	N ₁₈	-	27	0.0590 – 0.0964
	B	N ₁₆	N ₂₀	21	0.0920 – 0.1845
	A	N ₁₉	-	37	0.0964 – 0.4222
	C	N ₁₇	N ₂₀	20	0.3340 – 0.5665
720 MeV	B	N ₂₁	N ₂₅	47	0.0711 – 0.1564
	A	N ₂₅	-	46	0.1835 – 0.6761
	C	N ₂₄	N ₂₆	28	0.6536 – 0.7603
	B	N ₂₃	N ₂₆	27	0.2011 – 0.2520
	C	N ₂₂	N ₂₆	37	0.4729 – 0.7474
	B	N ₂₁	N ₂₆	36	0.1294 – 0.2435
855 MeV	B	N ₂₇	N ₃₁	35	0.3263 – 0.4378
	C	N ₂₈	N ₃₁	31	0.7300 – 0.9772
	A	N ₂₉	N ₃₀	32	0.3069 – 0.5011
	A	N ₂₉	-	13	0.5274 – 0.7656
	B	N ₂₇	N ₂₉	54	0.0868 – 0.3263

χ^2 equal to or lower than a bound regression as shown in Fig. 3 and Fig. 4 which plot the total χ^2 and charge radius given by the unbound and bound regressions of the 1422 Mainz cross section points and the 658 rebinned cross sections respectively. Since adding parameters will always either decrease or keep total χ^2 the same, χ^2 by itself is not a valid model selection criterion. More appropriate model selection techniques include using an F-Test for nested models [12, 27] or model selection methods like the Akaike Information Criterion (AIC) [28] or the Bayesian Information Criterion (BIC) [29] which can be used with non-nested models (see Ref. [30] for more

TABLE II. The values of the polynomial terms for the unbound and bound regressions of the 1422 cross section points following the notation of Eq. 3 and 4. If one wishes to interpret the charge form factor slope term ($i = 1$) in terms of charge radius using Eq. 2, one finds the unbound fit gives a charge radius of 0.882 fm while the bound fit gives a charge radius of 0.854 fm.

i	unbound		bound	
	a_i^E	a_i^M	a_i^E	a_i^M
1	-3.331	-2.523	-3.124	-2.800
2	13.05	-0.7081	8.821	5.188
3	-63.68	40.16	-25.74	-5.742
4	249.4	-176.7	60.06	2.806
5	-658.6	380.3	-89.41	0.0000
6	1099	-392.6	72.48	0.01034
7	-987.6	11.53	-24.23	-0.2766
8	57.38	442.4	0.0000	0.0000
9	853.4	-492.1	-0.0061	-0.0009
10	-810.5	230.3	0.0081	0.0013
11	250.4	-40.92	0.0000	0.0000

TABLE III. The values of the polynomial terms for the unbound and bound regressions following the notation of Eq. 3 and 4 for the 658 cross section points of rebinned data [13]. If one wishes to interpret the charge form factor slope term ($i = 1$) in terms of charge radius using Eq. 2, one finds the unbound fit gives a charge radius of 0.863 fm while the bound, continuously monotone fit gives a radius of 0.845 fm.

i	unbound		bound	
	a_i^E	a_i^M	a_i^E	a_i^M
1	-3.191	-2.465	-3.061	-2.760
2	10.83	-0.7271	8.413	4.979
3	-44.59	35.32	-24.46	-5.196
4	157.2	-136.4	58.23	2.193
5	-404.2	228.8	-89.36	0.0000
6	712.6	-98.11	74.77	0.5035
7	-733.1	-234.1	-25.73	-0.5330
8	133.4	349.9	0.0000	0.0000
9	632.8	-122.4	0.0000	0.0000
10	-695.5	-56.49	0.0000	0.0000
11	232.9	35.80	0.0000	0.0000

details). These statistical criteria are defined as follows:

$$\chi^2 = \sum_{n=1}^N ((data_i - model)/\sigma_i)^2, \quad (9)$$

$$AIC = N \log(\chi^2/N) + 2N_{\text{var}}, \quad (10)$$

$$BIC = N \log(\chi^2/N) + \log(N)N_{\text{var}}, \quad (11)$$

where N is the number of data points, $data_i$ and σ_i are measured values and estimated uncertainties, and N_{var} is the number of model parameters. With these criteria, the model with the lowest AIC or BIC value will be selected.

Further details about on model selection techniques can be found in [31].

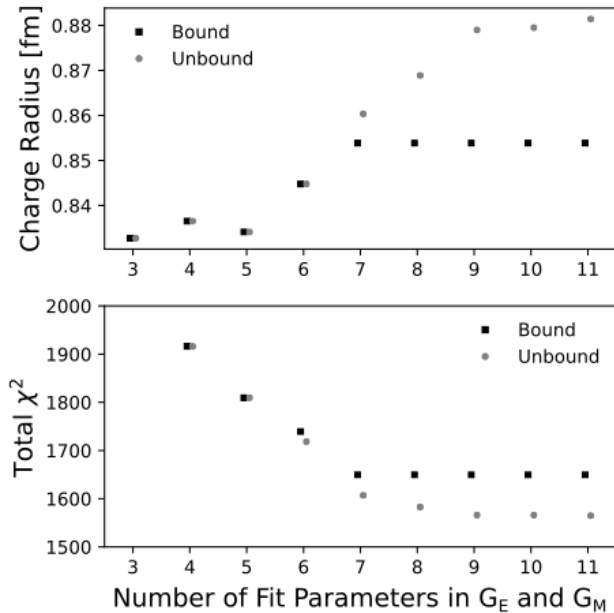


FIG. 3. Plotted is the total χ^2 for both the bound and unbound polynomial regressions of the full 1422 point Mainz dataset versus the number of fit parameters in G_E and G_M using Eq. 3 and 4. Total χ^2 continues to decrease as parameters are added, but at some point no significant improvement will be made where significance is defined using a statistics test such as an F-Test, AIC, and/or BIC [30]. Interestingly, the signs of the terms of both the bound and unbound fits both alternate until 7th order. With model selection using AIC or BIC, the bound fits should be stopped at 7th order while the unbound descriptive fits should be stopped at 10th.

One should also keep in mind whether one is trying to do a descriptive fit of the data or, by adding physical constraints, building a predictive or explanatory model of the data [2], while also keeping in mind that none of the model selection techniques will prevent the use of completely inappropriate functions. As noted in Ref. [32, 33], it is essential to plot the fit functions and residuals to ensure a reasonable regression as χ^2 values alone are insufficient.

As the changes we have presented in these four fits are larger than the statistical parameter uncertainties, we have limited ourselves to a discussion of the shifts of the mean values of the points. For non-linear regressions such as these, statistical bootstrapping can be used to find the statistical parameter uncertainties.

V. RESULTS

In Fig. 5 and Fig. 6, we show the individual electric and magnetic form factors obtained from the unbound and bound regressions for the 1422 Mainz cross section

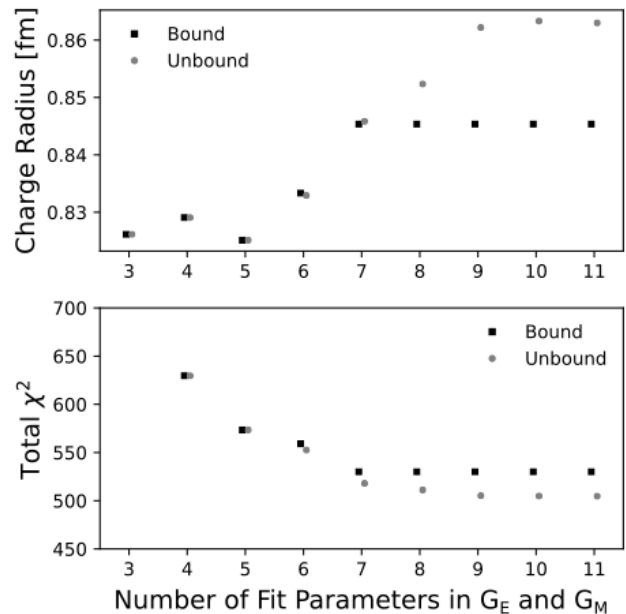


FIG. 4. Plotted is the total χ^2 for both the bound and unbound polynomial regressions of the 658 points of the rebinned Mainz dataset [13] versus the number of fit parameters in G_E and G_M using Eq. 3 and 4. It is disconcerting that with a reasonable rebinning of the data, the radius one would extract shifts for both the bound and unbound regressions. For these fits, by AIC and BIC, 7th order is the most appropriate for the bound regression while for the unbound 9th order is the most appropriate.

points. Though it is beyond the range of the data used in the regression, the results of regressions like these are frequently used to extract the charge radius of the proton by using Eq. 2 to relate the fit function to the charge radius of the proton. For the case of a polynomial, this is simply:

$$r_p = (-6a_1^E)^{1/2}, \quad (12)$$

and one finds a charge radius of 0.882 fm from the unbound regression and 0.854 fm from the bound. Thus, the radius extracted from the unbound regression is closer to the historically expected CODATA-2014 value while the radius extracted from the more physically justifiable bound regression is closer to the muonic results as well as the most recent atomic result [34]. With freedom to make analytic choices that so strongly affect the results, there is the potential for unconscious confirmation bias, and for researchers to select and report the regressions that confirm their expectations [25, 26].

VI. CONCLUSIONS

We have shown that small changes in analytic functions and binning choices applied to a complex non-linear

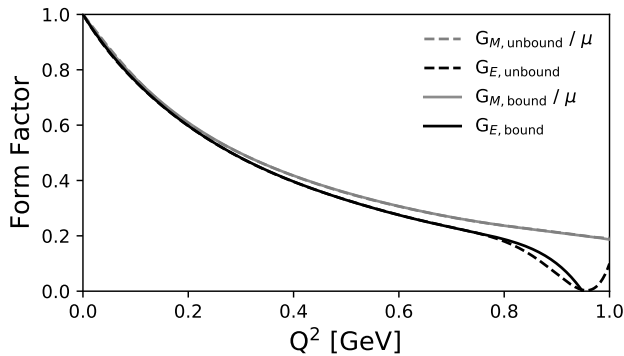


FIG. 5. Shown are the electromagnetic form factors from the unbound and bound polynomial regressions of the 1422 Mainz cross sections [20]. For these kinematics, as the Q^2 gets large, the cross sections are dominated by G_M and the G_E form factor becomes unconstrained, so the divergence at high Q^2 is to be expected from a high-order polynomial.

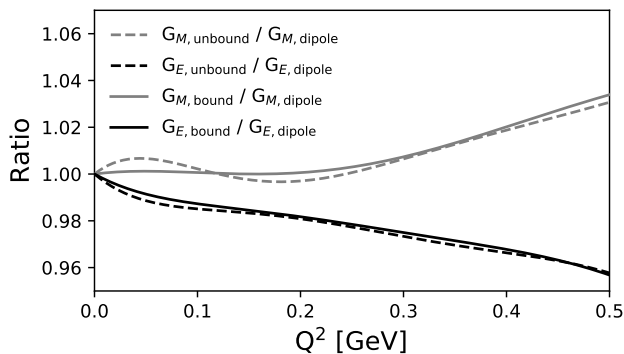


FIG. 6. The ratio of the extracted electromagnetic form factors to standard dipole for the 1422 Mainz cross sections show that the oscillation in the magnetic form factor goes away once the fit functions are forced to be continuously monotone. Interestingly, through a complex interplay with the normalization parameters, the smooth magnetic form factor also results in a smaller extracted proton radius (0.854 fm vs. 0.882 fm).

regression can result in significantly different results. In particular, using the Mainz data set of elastic cross section data, we have shown results consistent with the CODATA-2014 when using high-order unbounded polynomial fits and values close to the muonic results when using bounded polynomial regressions. Thus, by simply trying different functions, limits, and bounds, one can easily extrapolate to different results which can lead to confirmation bias and/or inappropriate rejection of certain results. Enrico Fermi noted that these types of problems should be addressed using either a firm mathematical basis or a physical model [35].

Thus, while one can argue that the bounded non-linear regressions is the more physical function, it would be more appropriate to approach the analysis such that the

analytic choices do not so strongly affect the results. To do this, one can either fit only lower Q^2 data where fewer free parameters are required [11, 12, 24, 30, 36–41] and the results are not sensitive to the magnetic form factor, as shown explicitly in Ref. [30]; or, as Fermi preferred, use a physical model, such as that of Bernard *et al.* [42] or Alarcón and Weiss [22] to constrain the fits [16, 17, 43, 44]. There are also the physically motivated functions such as rational functions [12, 45], continued fractions [11, 46, 47], or the z-expansion fits [13, 48] though these still require model selection techniques to determine the appropriate number of regression parameters. We hope to have illustrated that by using extremely complex non-linear regressions and deep searches, one can find nearly any radius in a wide range of radii from a single dataset [49]. To quote Nobel laureate Ronald H. Coase, “if you torture the data long enough, it will confess.”

ACKNOWLEDGMENTS

Many thanks to Franziska Hagelstein and Vladimir Pascalutsa for their questions about normalization parameters that prompted this work. Thanks to Dave Meekins for his many useful comments and discussions. Thanks to Nigel Tufnel for suggesting going to eleven. And thanks to Marcy Stutzman and Simon Širca for their editorial comments. This work was supported by the U.S. Department of Energy contract DE-AC05-06OR23177 under which Jefferson Science Associates operates the Thomas Jefferson National Accelerator Facility.

Appendix A: Robust Regressions

Ordinary least squares regression (OLSR) is one of the most commonly employed techniques used to fit a given model and its parameters to a dataset. However, OLSR is commonly misunderstood and misapplied by researchers. OLSR makes several key assumptions about the uncertainties of a dataset, most importantly that the uncertainties on the independent measurements are uncorrelated and normally distributed [23, 50]. When OLSR’s assumptions are not met, such as when the dataset has significant outliers, OLSR is not sufficient for fitting the data and can yield misleading results. To avoid these pitfalls, robust methods such as robust least squares regression (RLSR) should be used instead of OLSR techniques.

For OLSR, fit parameters are determined by minimizing the square of the differences between real-world data and model predictions. This is known as a χ^2 minimization, Eq. A1, for N data points with M fit parameters.

$$\chi^2 \equiv \sum_{i=1}^N \left(\frac{y_i - y(x_i | a_1, a_2, \dots, a_M)}{\sigma_i} \right)^2 \quad (\text{A1})$$

Here y_i are the measured data values, $y(x_i|a_1, a_2, \dots, a_M)$ are the values given by the model with fit parameters a_1 to a_M when evaluated at the x_i of the measured data, and σ_i are the uncertainties on each measured data point.

While OLSR via χ^2 minimization is often a useful initial method for checking the ‘goodness’ of a fit, it relies upon several important assumptions. OLSR is based on the core assumptions that the errors are random variables that are normally distributed, the errors are uncorrelated to each other, and the errors are homoscedastic, which is to say they have the same variance. Unfortunately, these assumptions rarely hold true in the case of real-world data. This causes OLSR to be overly influenced by even a single outlier [23, 50].

To avoid outliers having too much influence over a fit, we desire a method by which outliers can be identified and then re-weighted such that they do not skew the overall fit. The least squares minimization found in Eq. A1 can be generalized to Eq. A2 by introducing the function $\rho(z)$ [51]. OLSR is then simply the case where $\rho(z) = z$. Many functions can be used for $\rho(z)$ to introduce robustness, but for the following examples the ‘soft loss’ (softl1) function given in Eq. A3 was selected and implemented using the Python package SciPy [51–53].

$$\chi^2 \equiv \sum_{i=1}^N \rho_i(z) \quad \text{and} \quad z = \left(\frac{y_i - y(x_i|a_1, a_2, \dots, a_M)}{\sigma_i} \right)^2 \quad (\text{A2})$$

$$\rho(z) = 2(\sqrt{1+z} - 1) \quad (\text{A3})$$

With soft loss, as a z_i gets larger, the magnitude of $\rho_i(z)$ is increasingly reduced with respect to OLSR. A RLSR with soft loss essentially re-weights the outliers of a dataset, decreasing their influence when fitting. Note that if a dataset meets all of the above assumptions inherent to OLSR (i.e. errors are normally distributed, uncorrelated, and have the same variance) then OLSR and RLSR techniques should both produce the same fit results since the dataset, by definition, does not contain excessive outliers.

A simple example reproduced from a classic statistics paper [32] is shown in Fig. 7. The dataset has a single clear outlier which pulls the fit considerably away from the bulk of the data when using OLSR. However, when RLSR with soft loss is used to fit the data the influence of the outlier is greatly reduced, and the fit returns to the bulk of the data yielding superior results.

For a real-world example using RLSR we can study the full Initial State Radiation (ISR) dataset found in the supplemental material of Ref. [54, 55]. Fig. 8 shows the results of two regressions the proton electric form factor using the theory model of Alarcón and Weiss [22] with its single free parameter, the proton radius, with the data points and normalization from Ref. [54, 55]. The light

grey curve uses an OLSR to fit the dataset and the dark curve uses a RLSR with soft loss.

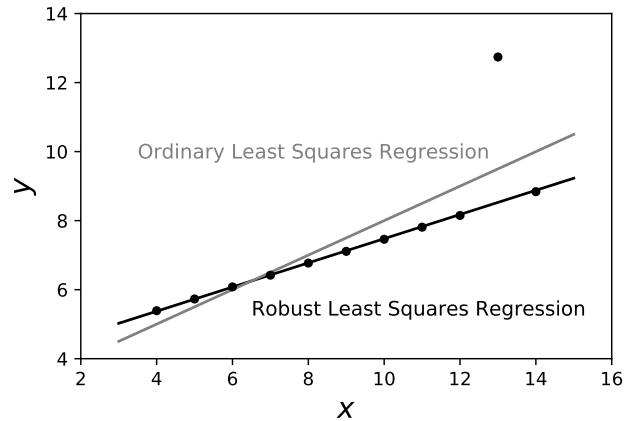


FIG. 7. This example data, reproduced from a classic statistics paper [32], shows how an OLSR is easily pulled away from the true trend of the data while a RLSR is only weakly affected by the outlier.

There is a clear separation between the two curves even using exactly the same data with the OLSR finding a radius of 0.874 fm and the RLSR finding significant smaller a radius of 0.844 fm. Again, the purely analytic choice of the regression type significantly influences the fit results. Further, the fact that OLSR and RLSR fit results differ significantly is evidence that there are outliers in the dataset that are not following a normal distribution, otherwise the OLSR and RLSR fits would have better agreement.

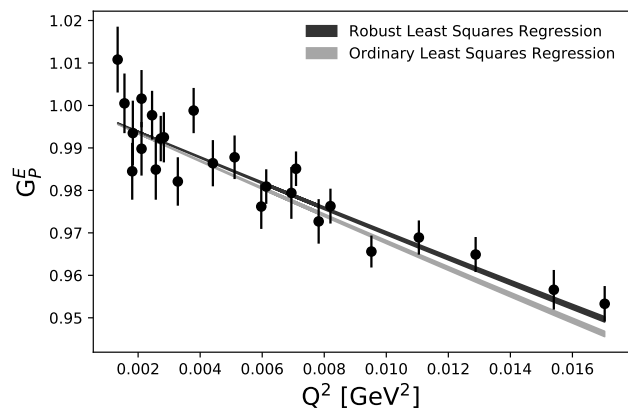


FIG. 8. Proton electric form factor data taken from the Initial State Radiation dataset found in the supplemental material of Ref. [54]. The uncertainties are calculated by summing the listed statistical uncertainties with the systematic uncorrelated uncertainties in quadrature. The theoretical model used for the regressions is the model of Alarcón and Weiss [22] with only one free parameter and gives a radius of 0.874 fm for the OLSR and 0.844 fm for the RLSR with soft loss.

- [1] R. Silberzahn *et al.*, *Advances in Methods and Practices in Psychological Science* **1**, 337 (2018).
- [2] G. Shmueli, *Statist. Sci.* **25**, 289 (2010).
- [3] R. Pohl *et al.*, *Nature* **466**, 213 (2010).
- [4] A. Antognini *et al.*, *Science* **339**, 417 (2013).
- [5] P. J. Mohr, D. B. Newell, and B. N. Taylor, *Rev. Mod. Phys.* **88**, 035009 (2016), arXiv:1507.07956 [physics.atom-ph].
- [6] R. Pohl, R. Gilman, G. A. Miller, and K. Pachucki, *Ann. Rev. Nucl. Part. Sci.* **63**, 175 (2013), arXiv:1301.0905 [physics.atom-ph].
- [7] C. E. Carlson, *Prog. Part. Nucl. Phys.* **82**, 59 (2015), arXiv:1502.05314 [hep-ph].
- [8] G. A. Miller, in *13th Conference on the Intersections of Particle and Nuclear Physics (CIPANP 2018) Palm Springs, California, USA, May 29-June 3, 2018* (2018) arXiv:1809.09635 [physics.atom-ph].
- [9] G. A. Miller, *Phys. Rev.* **C99**, 035202 (2019), arXiv:1812.02714 [nucl-th].
- [10] M. Horbatsch and E. A. Hessels, *Phys. Rev.* **C93**, 015204 (2016), arXiv:1509.05644 [nucl-ex].
- [11] K. Griffioen, C. Carlson, and S. Maddox, *Phys. Rev.* **C93**, 065207 (2016), arXiv:1509.06676 [nucl-ex].
- [12] D. W. Higinbotham, A. A. Kabir, V. Lin, D. Meekins, B. Norum, and B. Sawatzky, *Phys. Rev.* **C93**, 055207 (2016), arXiv:1510.01293 [nucl-ex].
- [13] G. Lee, J. R. Arrington, and R. J. Hill, *Phys. Rev.* **D92**, 013013 (2015), arXiv:1505.01489 [hep-ph].
- [14] K. M. Graczyk and C. Juszczak, *Phys. Rev.* **C90**, 054334 (2014), arXiv:1408.0150 [hep-ph].
- [15] I. T. Lorenz and Ulf.-G. Meißner, *Phys. Lett.* **B737**, 57 (2014), arXiv:1406.2962 [hep-ph].
- [16] M. Horbatsch, E. A. Hessels, and A. Pineda, *Phys. Rev.* **C95**, 035203 (2017), arXiv:1610.09760 [nucl-th].
- [17] J. M. Alarcón, D. W. Higinbotham, C. Weiss, and Z. Ye, *Phys. Rev.* **C99**, 044303 (2019), arXiv:1809.06373 [hep-ph].
- [18] S. Zhou, P. Giuliani, J. Piekarewicz, A. Bhattacharya, and D. Pati, *Phys. Rev.* **C99**, 055202 (2019), arXiv:1808.05977 [nucl-th].
- [19] J. C. Bernauer *et al.* (A1), *Phys. Rev. Lett.* **105**, 242001 (2010), arXiv:1007.5076 [nucl-ex].
- [20] J. C. Bernauer *et al.* (A1), *Phys. Rev.* **C90**, 015206 (2014), arXiv:1307.6227 [nucl-ex].
- [21] M. Merkle, in *Analytic Number Theory, Approximation Theory, and Special Functions*, edited by G. V. Milovanović and M. T. Rassias (Springer-Verlag New York, New York, 2012) Chap. 12, pp. 347–364, arXiv:1211.0900.
- [22] J. M. Alarcón and C. Weiss, *Phys. Lett.* **B784**, 373 (2018), arXiv:1803.09748 [hep-ph].
- [23] W. H. Press, S. A. Teukolsky, W. T. Vetterling, and B. P. Flannery, *Numerical Recipes 3rd Edition: The Art of Scientific Computing*, 3rd ed. (Cambridge University Press, New York, NY, USA, 2007).
- [24] X. Yan, D. W. Higinbotham, D. Dutta, H. Gao, A. Gasparian, M. A. Khandaker, N. Liyanage, E. Pasyuk, C. Peng, and W. Xiong, *Phys. Rev.* **C98**, 025204 (2018), arXiv:1803.01629 [nucl-ex].
- [25] J. J. Koehler, *Organizational Behavior and Human Decision Processes* **56**, 28 (1993).
- [26] J. P. A. Ioannidis, *PLOS Medicine* **2** (2005), 10.1371/journal.pmed.0020124.
- [27] S. Širca, *Probability for Physicists*, Graduate Texts in Physics (Springer International Publishing, 2016).
- [28] H. Akaike, *IEEE Transactions on Automatic Control* **19**, 716 (1974).
- [29] G. Schwarz, *Ann. Statist.* **6**, 461 (1978).
- [30] D. W. Higinbotham, P. Giuliani, R. E. McClellan, S. Sirca, and X. Yan, (2018), arXiv:1812.05706 [physics.data-an].
- [31] E. Wit, E. v. d. Heuvel, and J.-W. Romeijn, *Statistica Neerlandica* **66**, 217 (2012).
- [32] F. J. Anscombe, *The American Statistician* **27**, 17 (1973).
- [33] R. Andrae, T. Schulze-Hartung, and P. Melchior, arXiv e-prints, arXiv:1012.3754 (2010), arXiv:1012.3754 [astro-ph.IM].
- [34] N. Bezginov, T. Valdez, M. Horbatsch, A. Marsman, A. C. Vutha, and E. A. Hessels, *Science* **365**, 1007 (2019), <https://science.sciencemag.org/content/365/6457/1007.full.pdf>.
- [35] F. Dyson, *Nature* **427**, 297 EP (2004).
- [36] L. N. Hand, D. G. Miller, and R. Wilson, *Rev. Mod. Phys.* **35**, 335 (1963).
- [37] J. J. Murphy, Y. M. Shin, and D. M. Skopik, *Phys. Rev.* **C9**, 2125 (1974), [Erratum: *Phys. Rev.* **C10**, 2111 (1974)].
- [38] F. Borkowski, G. G. Simon, V. H. Walther, and R. D. Wendling, *Z. Phys.* **A275**, 29 (1975).
- [39] G. G. Simon, C. Schmitt, F. Borkowski, and V. H. Walther, *Nucl. Phys.* **A333**, 381 (1980).
- [40] F. Hagelstein and V. Pascalutsa, *Phys. Lett.* **B797**, 134825 (2019), arXiv:1812.02028 [nucl-th].
- [41] T. B. Hayward and K. A. Griffioen, (2018), arXiv:1804.09150 [nucl-ex].
- [42] V. Bernard, H. W. Fearing, T. R. Hemmert, and Ulf.-G. Meißner, *Nucl. Phys.* **A635**, 121 (1998), [Erratum: *Nucl. Phys.* **A642**, 563(1998)], arXiv:hep-ph/9801297 [hep-ph].
- [43] G. Hohler, E. Pietarinen, I. Sabba Stefanescu, F. Borkowski, G. G. Simon, V. H. Walther, and R. D. Wendling, *Nucl. Phys.* **B114**, 505 (1976).
- [44] I. T. Lorenz, Ulf.-G. Meißner, H. W. Hammer, and Y. B. Dong, *Phys. Rev.* **D91**, 014023 (2015), arXiv:1411.1704 [hep-ph].
- [45] J. J. Kelly, *Phys. Rev.* **C70**, 068202 (2004).
- [46] I. Sick, *Phys. Lett.* **B576**, 62 (2003), arXiv:nucl-ex/0310008 [nucl-ex].
- [47] I. T. Lorenz, H. W. Hammer, and Ulf.-G. Meißner, *Eur. Phys. J.* **A48**, 151 (2012), arXiv:1205.6628 [hep-ph].
- [48] R. J. Hill and G. Paz, *Phys. Rev.* **D82**, 113005 (2010), arXiv:1008.4619 [hep-ph].
- [49] D. W. Higinbotham, (2019), 10.5281/zenodo.2566639.
- [50] D. Draper, *Statistical Science* **3**, 239 (1988).
- [51] B. Triggs, P. F. McLauchlan, R. I. Hartley, and A. W. Fitzgibbon, in *Vision Algorithms: Theory and Practice*, edited by B. Triggs, A. Zisserman, and R. Szeliski (Springer Berlin Heidelberg, Berlin, Heidelberg, 2000) pp. 298–372.
- [52] E. Jones, T. Oliphant, P. Peterson, *et al.*, “SciPy: Open source scientific tools for Python,” (2001–), [Online; accessed 9/26/2019].

- [53] T. E. Oliphant, *Computing in Science & Engineering* **9**, 10 (2007).
- [54] M. Mihovilovi *et al.*, (2019), arXiv:1905.11182 [nucl-ex].
- [55] M. Mihovilović *et al.*, *Phys. Lett.* **B771**, 194 (2017), arXiv:1612.06707 [nucl-ex].